Micro-active control of a planar jet.

By TOM PEACOCK , ELIZABETH BRADLEY, JEAN HERTBERG , YUNG-CHENG LEE and VICTOR BRIGHT .

Department of Computer Science, University of Colorado at Boulder, Boulder, Colorado, 80309

(Received 9 December 2000)

We present the results of an experimental study in which a planar jet of air was forced by an array of micro-actuators. In the absence of any forcing, the mean velocity profile of the experimental jet was found to be in good agreement with theory. Thereafter, a natural instability of this jet was selectively excited using the micro-actuators.

---

1. Introduction

The prediction and control of fluid flows is a major research activity and the ability to do so, particularly in aerospace and combustion applications, can generate huge financial and environmental savings. To date, most experimental studies of flow control have been performed using conventionally machined actuators (Wiltse & Glezer 1993; Fan, Herbert & Haritonides 1995; Jacobson & Reynolds 1998; Wiltse & Glezer 1998). Recently, however, there has been much interest in using MEMS†-based technology for flow control, as it offers several advantages over conventional machining, such as batch processing of devices on the micron scale. A review of the use of MEMS devices for flow control is given by Ho & Tai (1998) and Löfdahl & Gad-el-Hak (1999).

† Micro Electro Mechanical Systems

In this paper, we present the results of an experimental study of flow control of a low Reynolds number planar jet of air using MEMS micro-actuators. In this preliminary study, we were able to selectively enhance a natural instability of the jet by providing small-amplitude velocity perturbations at its source. The two-dimensional flow geometry is an idealised situation about which much has been written, and we chose this arrangement to make the system amenable to analysis and numerical simulation. A summary of the relevant theory is presented in the following section. The experimental jet facility and the MEMS actuators are then described. Thereafter we present results from the experiment and show that the micro-actuators were able to excite an instability of the jet.

2. The planar jet

The planar jet is a two-dimensional laminar jet. It can be realised in an experiment by considering a cross section of the flow out of a very long thin slit. The velocity profile of a planar jet, first obtained by Bickley (1937), gives an accurate description of two-dimensional jet flow provided one is not too close to the source of the jet. A sketch of the streamlines of a planar jet is presented in figure 1. These are everywhere parallel to the local flow, and arrowheads have been drawn on the streamlines to indicate the flow direction. To show the magnitude of the velocity along the streamlines, graphs of the velocity profile at several downstream locations have been superimposed. The Bickley profile has been observed experimentally by Andrade (1939) and Sato & Sakao (1964), among others. The latter noted that the velocity profile was initially parabolic, because the flow passed through a parallel channel before reaching the exit slit, and evolved into that of a Bickley jet further downstream.

A planar jet is unstable when the Reynolds number, based on the width and peak

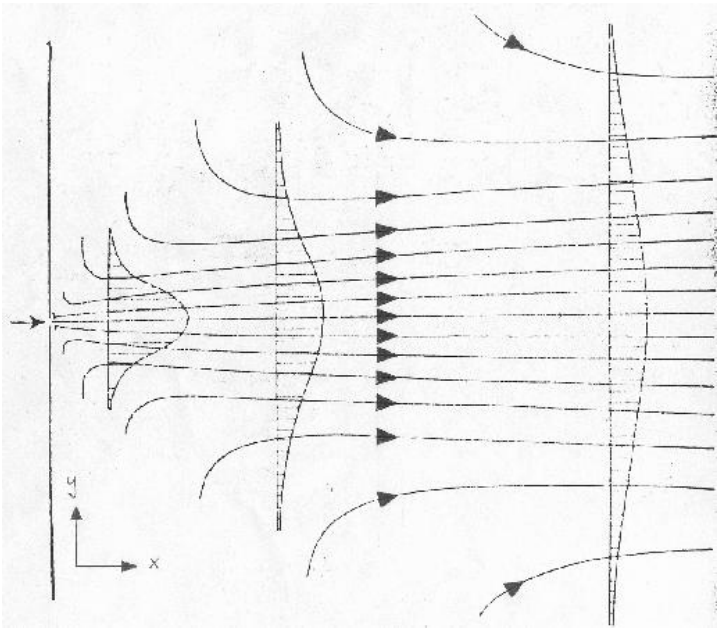

FIGURE 1. Streamlines and velocity profiles for the planar jet. This sketch is taken from the paper by Bickley (1937).

velocity of the jet, is of the order of 10. Small-scale velocity disturbances, which arise naturally in any experiment, are amplified as they move downstream and can generate large-scale flow structures that dominate the flow field. Stability analysis shows that the planar jet is unstable to two different types of velocity disturbance, one symmetric about the jet centreline and the other antisymmetric (Savic 1941; Lessen & Fox 1955; McKoen 1957; Curle 1957; Howard 1958; Tatsumi & Kakutani 1958; Clenshaw & Elliot 1960). The disturbances travel as a wave along the jet, with a characteristic wavelength and frequency. Velocity profiles of the two modes are presented in figure 2. The perturbation velocity of the symmetric mode has a maximum on the jet centreline; oscillations on either side of the centreline are in phase. In contrast, the amplitude of fluctuation is zero on the jet centreline for the antisymmetric mode, and oscillations on either side are in anti-phase. When a velocity perturbation is applied to the planar jet, it can excite these two spatial modes of instability. This effect was first reported by Brown (1935), who was

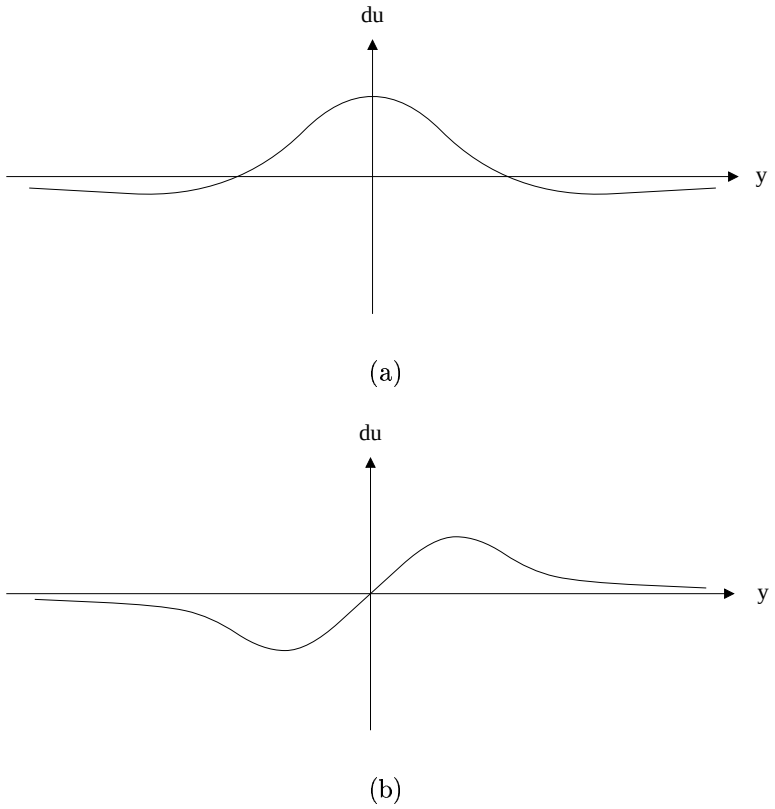

FIGURE 2. Velocity profiles of the unstable modes of a planar jet, where du is the perturbation velocity. (a) Symmetric mode. (b) Antisymmetric mode.

interested in the phenomenon of sensitive flames (Leconte 1858), but it was Sato (1960) and Sakao & Sato (1964) who first directly observed these modes in a planar jet, using sound waves to provide a disturbance. In the experiments of Sato (1960) and Sato & Sakao (1964) the observed values of the amplification rate and propagation velocity of these disturbances were found to be in good agreement with theoretical predictions of Lessen & Fox (1955) and Tatsumi & Kakutani (1958). The amplification of disturbances by a jet is of great importance in engineering applications, such as combustion and mixing processes, and one of the goals of this project is to learn how to control and exploit them.

3. The experiment

Achieving control of a planar jet is very difficult because of the instabilities described in the previous section. An additional problem arises because the flow field in an experiment is nominally two-dimensional. In practice, one considers a cross section of flow from a long, thin slit, but any such flow will become three-dimensional downstream from the source. This is because the exit slit is of finite length, so that end effects are important, and also due to unavoidable three-dimensional disturbances from the surroundings. Eventually, we intend to turn this to our advantage, as it provides a means for controlling three-dimensional flow structures using actuators arrayed along a single axis of the flow. Since the initial investigations reported here are concerned with two-dimensional flow, the exit slit was made extremely long to minimise end effects. Furthermore, Lasheras (1988) showed that three-dimensional instabilities, excited by disturbances from the surroundings, will not couple with two-dimensional instabilities in the near-field region of the jet. This means we can investigate two-dimensional flow in this region, confident that three-dimensional effects are not important.

A schematic of the experiment is presented in figure 3(a). The experiment was designed and constructed with the aid of Jean Hertzberg. The exit slit was 400mm long and 2.5 $\pm$ 0.01mm wide. It was defined to be in the y-z plane, as shown in figure 3(b), with the longer side along the z-axis. Below the exit slit was a plenum section and a contraction section. Compressed air was filtered and entered the base of the plenum through an array of hoses. The air passed upwards through fine wire mesh screens that reduced the level of turbulence in the flow. Upon reaching the top of the plenum, the air then passed through a matched cubic contraction of area ratio 6 to 1, which further reduced turbulence, and left the plenum through the exit slit. The experiment was highly sensitive to both

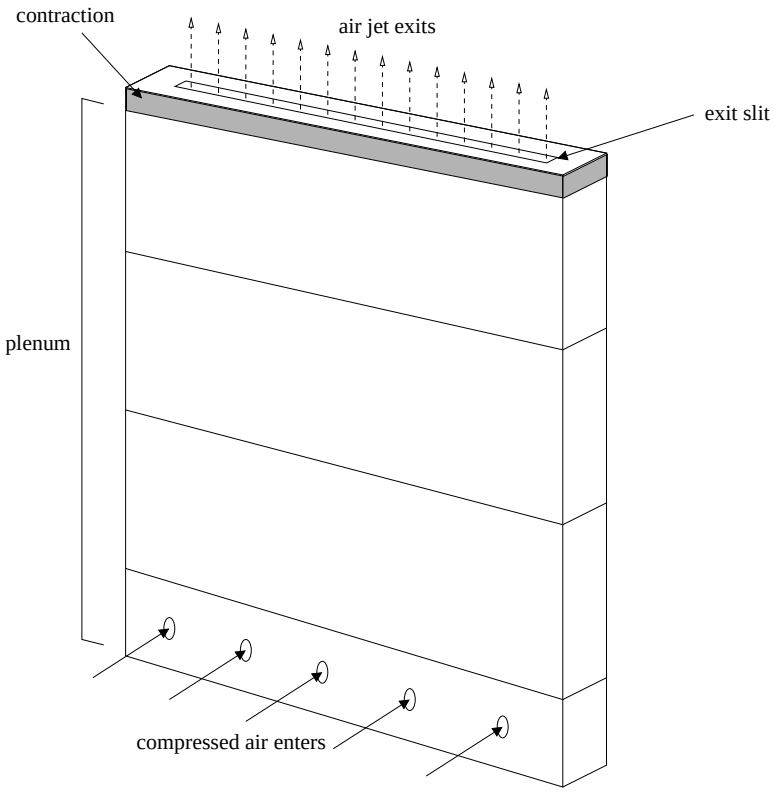

(a)

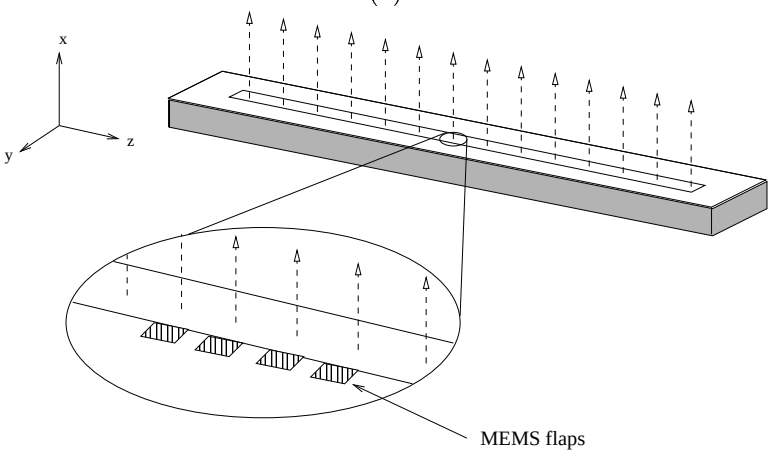

(b)

FIGURE 3. (a) Schematic of the experiment showing the exit slit, and the plenum and contraction sections. (b) The exit slit, with four MEMS actuators placed along the centre of one side.

mechanical vibrations and motion of the ambient air, so it stood on vibration control mounts and was enclosed by isolation screens.

The flow emerging from the exit slit was investigated in two ways. Detailed flow measurements were made with a hotwire anemometer, which measures the magnitude of the velocity by recording the electrical resistance of a heated thin wire suspended in the flow. The resistance changes as the air cools the wire, hence the name of the method. The hotwire probe was mounted on translation stages and could be moved in the streamwise (x) direction and cross-stream (y) direction with an accuracy of 0.025mm. The hotwire was calibrated using a low-speed windtunnel and was operated by a constant temperature method. Its output was digitised using a 12-bit A/D converter and analysed using commercial LabView software. Hotwire measurements of both mean and fluctuating velocity profiles were made in the $x - y$ plane across the centre of the exit slit. The peak velocity at the exit slit was in the range from 0.3 to 1.5m/s, giving a range of Reynolds numbers from 50 to 250, based on the peak velocity at the exit slit, u_{00}, the slit width, d, and the kinematic viscosity of air, ν. For the velocities considered, the flow was found to be uniform across the length of the exit slit, showing that the emerging jet was indeed two dimensional. Large-scale qualitative images of the flow were obtained by seeding the air supply with fine oil droplets and illuminating the jet with a sheet laser beam. These images proved useful for observing the downstream effects of small perturbations near the nozzle.

External forcing of the jet was provided by an array of four MEMS actuators positioned on one side of the exit slit, as shown in figure 3(b). The individual actuators were polysilicon flaps 1mm long and 0.25mm wide that moved under the influence of an applied voltage. The actuators were designed with the help of Victor Bright's research group at the University of Colorado and were fabricated using the commercial MUMPS surface

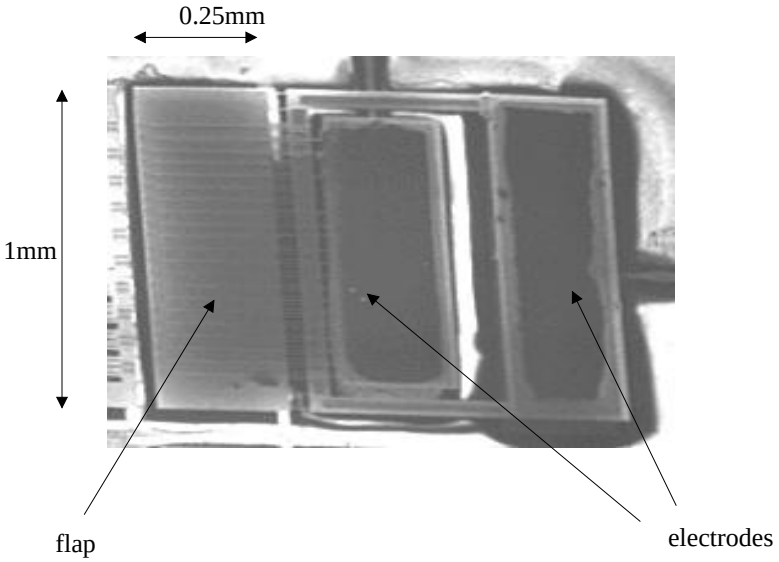

FIGURE 4. A single MEMS actuator. The actuating flap is on the left of the image and the electrode connections are on the right.

micro-machining process with the aid of Y.C. Lee and his research group. An electron microscope image of one of these MEMS actuators is presented in figure 4, in which the MEMS device appears as a dark grey structure. The actuating flap is on the left of the image and there are two electrode connections, one in the centre and the other on the right. The device was constructed from two layers of polysilicon of different thicknesses and operated using the bi-layer effect (Gad-el-Hak 1999). That is to say that passing a current through the two layers of polysilicon caused them to be differentially heated and expand by different amounts, which caused the structure to deflect. The resonant frequency of an actuator† was around 25Hz, as can be seen from the results presented in figure 5(a). For a driving voltage of 5 volts, the tip of the flap had a displacement of 10 microns at 25Hz. Above 25Hz, the displacement amplitude decreased significantly with increasing frequency to a value of about 4 microns at 200Hz. By fixing the driving

† the frequency at which a given imposed voltage elicits the largest response

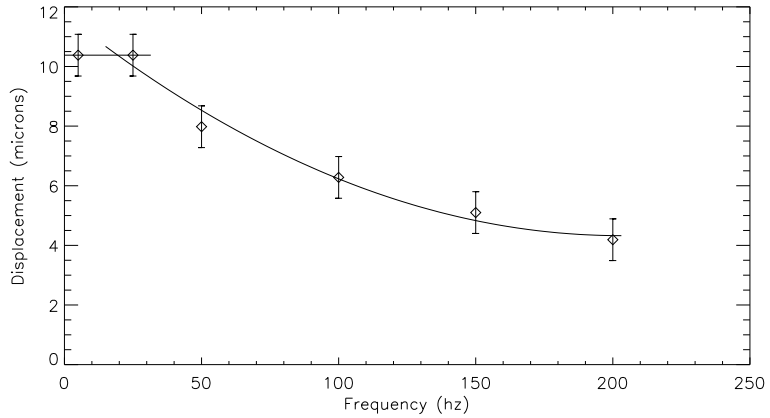

(a)

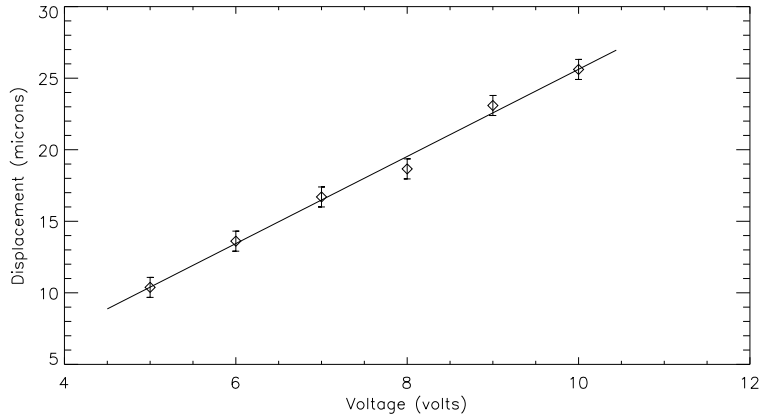

(b)

FIGURE 5. Response characteristics of the MEMS actuators. (a) The tip deflection as a function of frequency for an applied a. c. voltage of 5 volts. Above 25Hz, the amplitude of displacement decreases significantly. (b) The tip deflection as a function of applied a. c. voltage for a driving frequency of 25 Hz.

frequency at 25Hz and increasing the applied voltage, the maximum deflection that could be obtained was of the order of 25 microns, as shown in figure 5(b). Above this voltage the flap suffered permanent damage. The velocity perturbation provided by these flaps, obtained by multiplying the amplitude of deflection by the driving frequency, was in the range 0.05 to 1 mm/s for the voltage and frequency ranges considered.

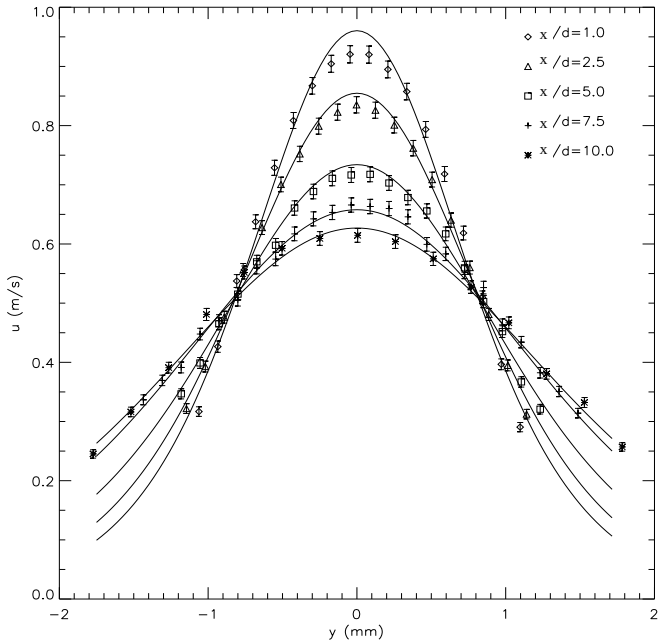

FIGURE 6. Mean velocity distributions for Re = 153. Results have been plotted for several downstream positions. x/d is the downstream location divided by the exit slit width $d = 2.5\mathrm{mm}$. A velocity profile of the Bickley jet (the solid curves) has been fitted to each set of results.

4. The mean velocity distribution

Figure 6 shows mean velocity distributions measured by the hotwire anemometer at several different downstream locations, in the absence of any MEMS forcing. In this figure, x/d is the downstream position nondimensionalised by the width of the exit slit. The velocity at the centre of the exit slit was 0.91m/s, corresponding to a slit Reynolds number of 153. As expected, the velocity on the centreline of the jet decreases and the width of the jet increases downstream. Solid curves drawn through the data points are fitted velocity profiles of the form predicted by Bickley. Near the exit slit, the velocity profile differs from the theoretical form, as shown by the offset between data points and the fitted curve. In this region, the flow is more parabolic in nature, a characteristic

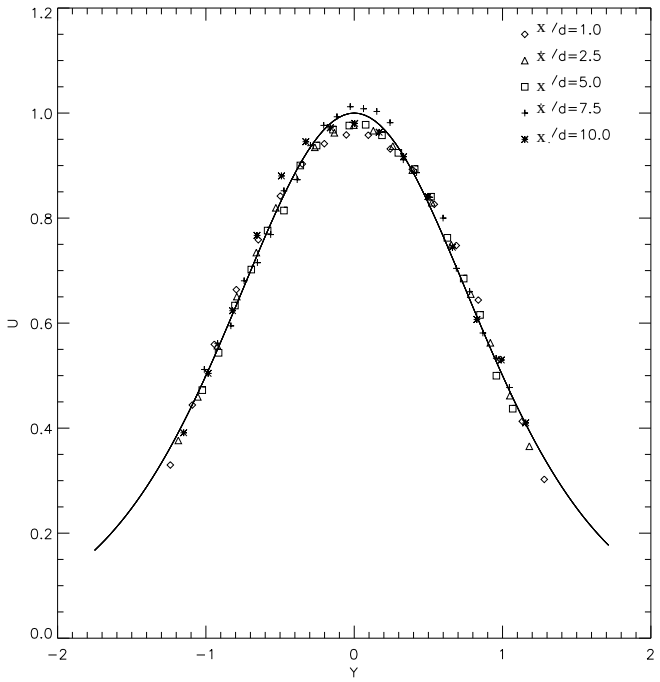

FIGURE 7. Nondimensionalised mean velocity distributions demonstrating the agreement between experiment and theory. U = u/u_0 is the nondimensional streamwise velocity and Y = y/b is the nondimensional cross-stream position. The solid line is the dimensionless profile for a Bickley jet.

of fully developed flow†. Further downstream, however, the velocity profile is seen to develop into that of the Bickley jet, and the data points agree very well with the fitted curves.

Similarity, an important feature of planar jet flow, requires that the velocity profile has the same geometrical form at each downstream location. The similarity of our experimental jet is demonstrated in figure 7, in which the velocity measurements presented in figure 6 have been nondimensionalised by the maximum speed u_0 at each downstream location and the cross-stream position y has been nondimensionalised by the half-width

† fully developed flow is that obtained at low Reynolds numbers in a channel with parallel walls. For example see Tritton, pages 7-11

of the jet b‡. It can be seen that the individual profiles fall on top of one another, demonstrating geometrical similarity. Moreover, they agree well with the theoretical profile of Bickley, which is the solid line drawn through the data.

An alternative way to show agreement between experiment and theory is to consider the variation of the peak velocity, u_0, and the jet halfwidth, b. Bickley predicted that u_0^3 and $b^{\frac{3}{2}}$ should both be proportional to the downstream position. The experimental results presented in figure 8 are in good agreement with this theory. The lines fitted to the experimental data were obtained using a nonlinear least squares fit, and both intersect the abscissa near x/d = -3†. This point of intersection is referred to as the virtual origin of the jet; it is the location of a point source of momentum from which the jet can be considered to originate. It is different from the location of the exit slit, which is referred to as the geometrical origin. This difference arises because the exit slit has finite width and, moreover, the velocity distribution at the slit is not of jet type but parabolic.

5. Control of Instability

As described in section 2, the planar jet is known to be unstable to two different types of disturbance when the Reynolds number is of the order of 10, one symmetric about the centreline of the jet and the other antisymmetric. Of these, the latter is more unstable, and therefore most likely to arise in an experiment.

At Re = 153 our experimental planar jet was unstable; figure 9(a) shows a section of a time series of streamwise velocity fluctuations obtained away from the centreline at x/d = 7.5. The amplitude of the fluctuations was of the order of 10mm/s. The variation in

‡ this being the distance from the centreline to the point at which $u/u_0 = 1/2$.

† The data at $x/d = 1.0$ was not used in the fitting as the velocity profile was parabolic and thus not of jet type.

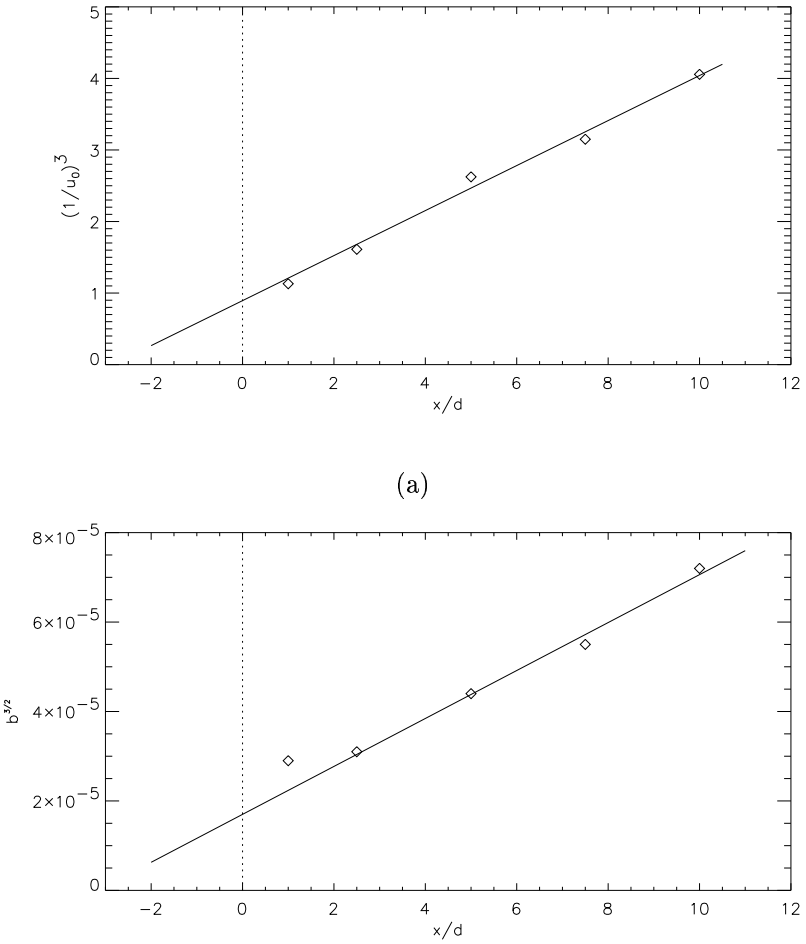

FIGURE 8. (a) The variation of peak velocity with downstream position. (b) The variation of jet halfwidth with downstream position.

amplitude arose because the fluctuations were initiated by unavoidable disturbances in the surrounding air, whose amplitudes varied in a random manner. The frequency of the jet fluctuations was 16.83Hz, as shown by the Fourier spectrum presented in figure 9(b), and this did not vary in either the x or y direction. In this case, the frequency of the fluctuations corresponded to a vibration in the experimental system which has since been

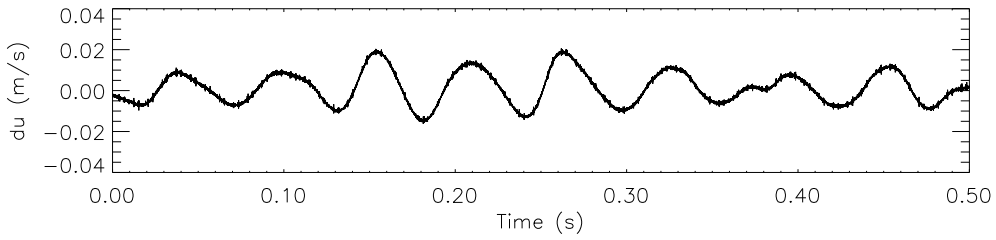

(a)

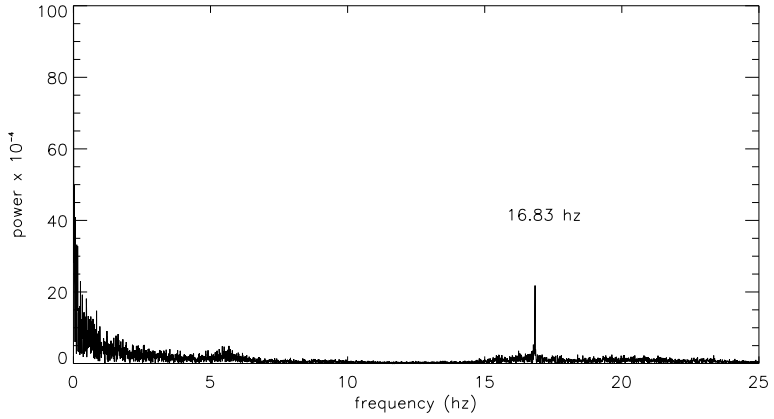

(b)

FIGURE 9. (a) Time series of streamwise velocity fluctuations at x/d = 7.5, where du is the deviation of the streamwise velocity about the mean value. (b) FFT of the time series in part (a).

eliminated. More generally, the growth rate of an instability is a function of frequency and one expects to observe fluctuations at the frequency with the highest growth rate.

It is not possible to determine from a single time series whether the observed fluctuations are the result of a symmetric or antisymmetric instability. To determine this, one has to traverse the flow and observe the spatial variation of the fluctuations. The characteristic feature of the antisymmetric instability, as described above, is that the amplitude of fluctuations is zero on the jet centreline with a maximum on either side (Savic

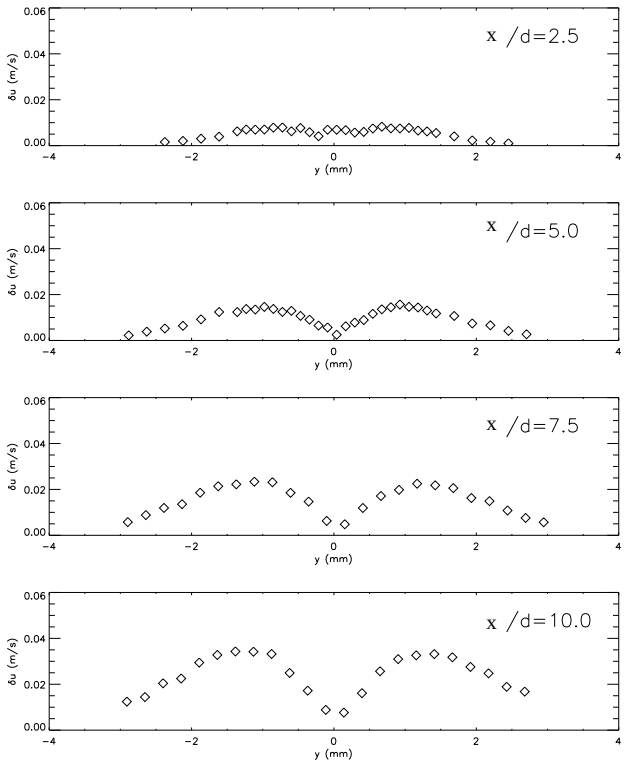

FIGURE 10. Graphs of the RMS amplitude of fluctuation at several downstream locations for the unforced jet. This corresponds to the antisymmetric instability of a planar jet, for which fluctuations are zero on the jet centreline and have a maximum on either side.

1941). The RMS† amplitudes of these fluctuations, measured at several downstream positions, are presented in figure 10. These graphs show that the RMS fluctuation amplitude increased with downstream position, and that the distribution had a minimum on the centreline and a peak on either side. This behavior is consistent with the antisymmetric instability of a jet, with one important point of note; fluctuations on either side of the centreline are in anti-phase for the antisymmetric instability, but our results contain no phase information about the disturbances because of the RMS averaging. In contrast, for

† Root-Mean-Square

the symmetric instability of a planar jet, the RMS amplitude of fluctuation is expected to be maximum on the centreline, and fluctuations on opposite sides of the centreline are in phase.

Control of the instability of the jet by introduction of artificial disturbances was investigated using the array of micro-actuators positioned along the exit slit. As described in section 3, these provided a localised velocity disturbance on one side of the jet. As an initial experiment, we decided to further excite the dominant mode at Re = 153 by forcing the actuators at 16.83Hz. The amplitude of forcing was of the order of 0.2mm/s (see figure 5). Figure 11(a) shows a portion of a time series of the resulting streamwise velocity fluctuations. Note the difference between this time series and that presented in figure 9 for the unforced jet; the forced response is highly sinusoidal and much larger in amplitude. This difference is even more apparent in the frequency domain, as shown in part (b) of the figure. The amplitude of the peak at 16.83Hz is much greater than the corresponding peak in the unforced jet (figure 9(b)). To ascertain that this was indeed the result of the antisymmetric instability, we plotted the RMS amplitude of fluctuation at several downstream positions, as shown in figure 12. As in figure 10, the amplitude of fluctuation was again smallest on the jet centreline, with a peak on either side, which is consistent with the antisymmetric instability. In contrast to the unforced jet, however, the peaks on either side were much larger and of different amplitude. This reflects the influence of the micro-actuators, which caused the RMS amplitude to initially be much larger on the side of the jet that was subject to forcing. It is interesting to note that the jet flow naturally corrects this imbalance as it moves downstream, so that by $x/d = 10$ the distribution is almost even.

To demonstrate that we could selectively excite the natural instability at other frequencies, we forced the jet at 5Hz and 50Hz, at amplitudes of 0.05mm/s and 0.5mm/s,

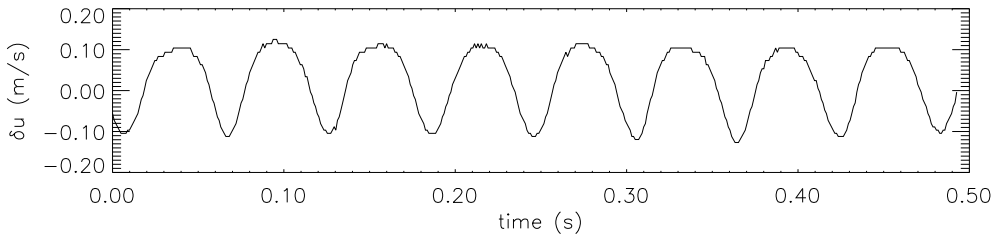

(a)

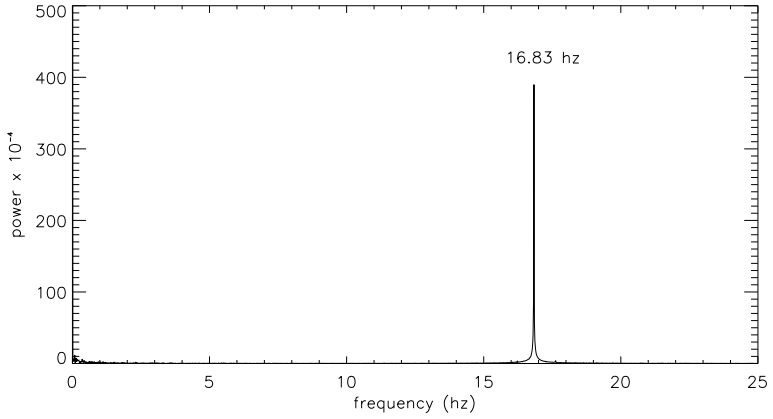

(b)

FIGURE 11. (a) Time series of streamwise velocity fluctuations for the excited jet at x/d = 7.5, where du is the deviation of the streamwise velocity about the mean value. (b) FFT of the time series in part (a).

respectively. Figure 13 shows Fourier spectra of the resulting behavior. In both cases, there is a smaller peak at 16.83Hz, corresponding to the preferred transition frequency of the jet, and a much stronger peak at the frequency at which the jet was being forced. The peaks for forcing at 5Hz and 50Hz differ in amplitude for two reasons; the growth rate

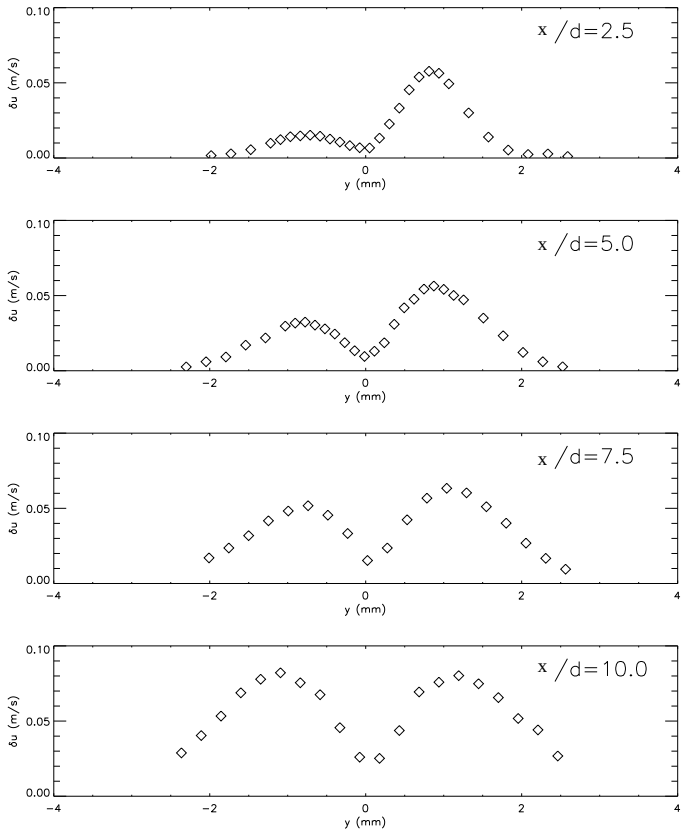

FIGURE 12. Graphs of the RMS amplitude of fluctuation at several downstream locations for the forced jet.

depends on the frequency† and the forcing amplitude was different due to the frequency response of the MEMS actuators.

The results presented above are concerned with the region close to the exit slit. It is well known that if small-scale disturbances described are further amplified as they progress downstream, large-scale vortex motion can arise. This is demonstrated experimentally by the two images presented in figure 14, which were taken at Re $\sim$ 50. The left-hand

† For a given Reynolds number jet, there is a frequency range outside of which disturbances are no longer amplified and are in fact suppressed (Curle, 1957).

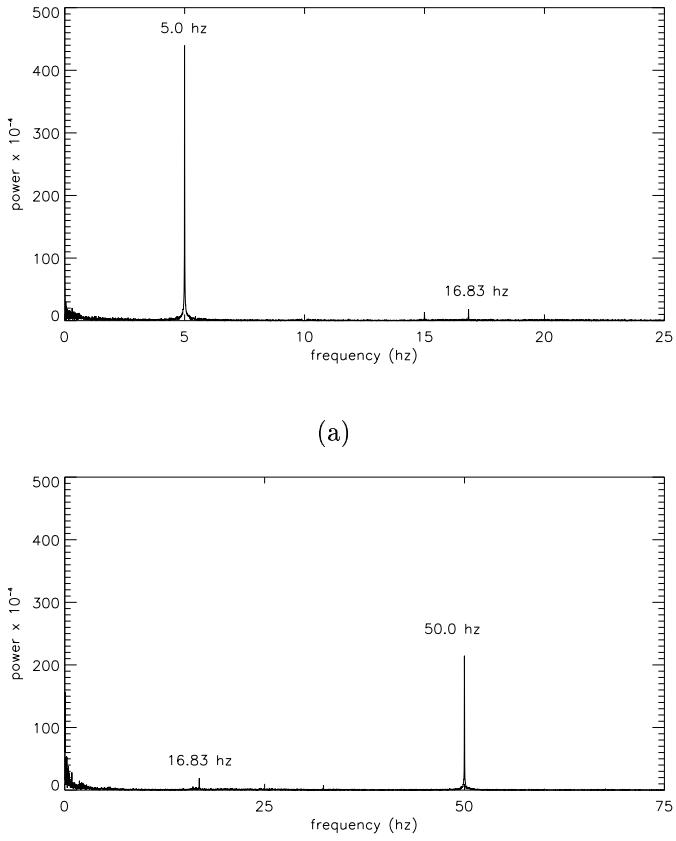

FIGURE 13. Fourier spectra of time series. (a) 5Hz excitation frequency. (b) 50Hz excitation frequency.

image shows the unforced jet flow; in the right-hand image, the micro-actuators were moving with a frequency of 6Hz. These images were obtained by seeding the flow with fine oil droplets and illuminating it with a sheet laser oriented perpendicular to the exit slit, in the $x - z$ plane. The domain shown in each image is approximately 10cm wide and 15cm tall. The device for positioning the micro-actuators can be seen in the lower right hand corner, although the MEMS themselves cannot be seen on this scale. The

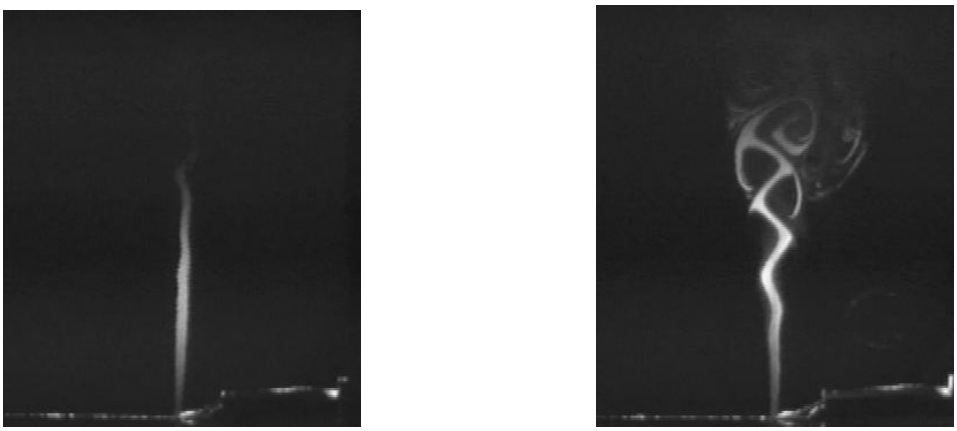

(a) (b)

FIGURE 14. Flow visualisation at at Reynolds number of approximately 50. (a) The unforced jet. (b) The jet forced at a frequency of 6Hz.

image in figure 14(a) shows unforced jet flow. Small-amplitude fluctuations that were detected using a hotwire (e.g., figure 11(a)) cannot be observed using the sheet laser flow visualisation. It is clear, however, that there are no obvious large-scale vortices present in the unforced flow. In contrast, the image in figure 14(b) shows the response of the same jet to forcing at a frequency of 6Hz. The small-amplitude fluctuations produced by the micro-flaps have been amplified greatly by the flow, and nonlinear effects have given rise to a roll up of large-scale vortices that dominate the flow field. A significant effect of these vortices is that they entrain a great deal of ambient air into the jet. Our long-term goal is to use the micro-actuators to control the dynamics of these large-scale structures, which has direct application to combustion and other processes where mixing is important.

6. Conclusions and further work

The response of a planar jet of air to external excitation has been investigated using an array of MEMS micro-actuators. In the absence of any excitation, the mean velocity profile of the jet was found to be in good agreement with theoretical predictions. In particular, the mean velocity profile was unstable to antisymmetric disturbances, and we were able to selectively excite this instability at a range of different frequencies using the MEMS micro-actuators.

The experiments described here are the first step in a research program whose goal is to establish complete control of the dynamics of a planar jet. At present, we are improving the isolation chamber in which the experiment is housed, so as to further reduce the influence of random disturbances. The next significant step is to mount MEMS micro-actuators on *both* sides of the exit slit, enabling us to excite both the antisymmetric and symmetric instabilities of this low Reynolds number planar jet. This kind of control, something that has not previously been achieved, will be accomplished by driving the actuators on either side of the slit in anti-phase and in phase, respectively. We shall then measure characteristics of both instabilities, such as the spatial growth rate of disturbances at different Reynolds numbers, and make comparisons with theory. Thereafter, we aim to apply closed-loop techniques to the jet, enabling selective enhancement and suppression of the two instabilities.

REFERENCES

ANDRADE, E. N. DA C. 1939 The velocity distribution in a liquid-into-liquid jet. Part 2 : The plane jet. *Proc. Phys. Soc.* **51**, 784–793.

BICKLEY, W. G. 1937 The plane jet. *Phil. Mag.* **23**, 727–731.

BROWN, G. B. 1935 On vortex motion in gaseous jets and the origin of their sensitivity to sound. *Proc. Phys. Soc.* **47**, 703–731.

CLENSHAW, C. W. & ELLIOT, D. 1960 A numerical treatment of the Orr-Sommerfeld equation in the case of a laminar jet. *Quart. J. Mech. Appl. Math.* **13**, 300–313.

CURLE, N. 1957 On hydrodynamic stability in unlimited fields of viscous flow. *Proc. Roy. Soc. A* **238** 489–501.

FAN, X. , HERBERT, T. & HARITONIDIS, J. H. 1995 Transition control with neural networks. *AIAA 33rd Aerospace Sciences Meeting, Report 95-0674*

HO, C-M. & TAI, Y-C. 1998 Micro-electro-mechanical-systems (MEMS) and fluid flows *Ann. Rev. Fluid Mech.* **30**, 579–612.

HOWARD, L. N. 1958 Hydrodynamic stability of a jet. *J. Math. Phys.* **37**, 283–298.

JACOBSON, S. A. & REYNOLDS, W. C. 1998 Active control of streamwise vortices and streaks in boundary layers. *J. Fluid Mech.* **360**, 179–211.

LECONTE, J. 1858 On the influence of musical sounds on the flame of a jet of coal gas. *Phil. Mag.* 4^{th} ser. XV, 235.

LEE, G. B. , HO, C-M. , JIANG, F. , LIU, C. , TSAO, T., *et al* 1996 Control of roll moment by MEMS. *ASME DA. Los Angeles : UCLA.*

LÖFDAHL, L. & GAD-EL-HAK, M. 1999 MEMS applications in turbulence and flow control. *Prog. Aero. Sci.* **35**, 101–203.

LASHERAS, J. C. & CHOI, H. 1988 3-dimensional instability of a plane free shear-layer - an experimental study of the formation and evolution of streamwise vortices. *J. Fluid Mech.* **189**, 53.

LESSEN, M. & FOX, J. A. (1955) *Jahre Grenzschichtforschung* (eds. H. Görtler & W. Tollmien) **50** 122

MCKOEN, C. H. 1957 *Aero. Res. Coun. Lond.*, current paper No. 303.

SAVIC, P. 1941 On acoustically effective vortex motion in gaseous jets. *Phil. Mag.* **32**, 245–252.

SATO, H. 1960 The stability and transition of a two-dimensional jet. J. Fluid Mech. **7**, 53–83.

SATO, H. & SAKAO, F. 1964 An experimental investigation of the instability of a two-dimensional jet at low Reynolds numbers *J. Fluid Mech.* **20**, 337–352.

TRITTON, D. J. 1988 *Physical Fluid Dyamics,* Oxford.

TATSUMI, T. & KAKUTANI, T. 1958 The stability of a two-dimensional laminar jet. *J. Fluid Mech.* **4**, 261–275.

WILTSE, J. M. & GLEZER, A. 1993 Manipulation of free shear flows using piezoelectric actuators. *J. Fluid Mech.* **249**, 261–285.

WILTSE, J. M. & GLEZER, A. 1998 Direct excitation of small scale motions in free shear flows. *Phys. Fluids* **10**, 2026–2036.